Hindawi
Geofluids
Volume 2021, Article ID 5512729, 16 pages
https://doi.org/10.1155/2021/5512729

Research Article

Evaluation of the Water Yield of Coal Roof Aquifers Based on the FDAHP-Entropy Method: A Case Study in the Donghuantuo Coal Mine, China

Yaowen Zhang,[1,2] **Lili Zhang**,[2] **Haijun Li**,[2] **and Baoming Chi**[2]

[1]*Key Laboratory of Earthquake Engineering and Engineering Vibration, Institute of Engineering Mechanics, China Earthquake Administration, Harbin, Heilongjiang 150080, China*
[2]*School of Ecology and Environment, Institute of Disaster Prevention, Sanhe, Hebei 065201, China*

Correspondence should be addressed to Lili Zhang; zhanglili@cidp.edu.cn

Received 26 February 2021; Revised 23 April 2021; Accepted 3 May 2021; Published 24 May 2021

Academic Editor: Guanglei Zhang

The water yield of coal seam roof aquifers is the key factor for evaluating and controlling water disasters in coal seam roofs. To evaluate the water yield of the sandstone aquifer in the roof of the Carboniferous-Permian Damiaozhuang Formation no. 8 coal seam in the Donghuantuo Mine, North China, seven main controlling factors affecting the water yield of sandstone aquifers are determined, including the permeability coefficient, consumption of drilling fluid, core recovery, aquifer thickness, brittle-plastic rock thickness ratio, fault scale index, and fault point density. Further, the fuzzy Delphi analytic hierarchy process (FDAHP) and entropy weight method (EWM) are used to calculate the subjective and objective weights of each main factor, respectively, and a combination weight model (CWM) is proposed based on the least square method to compose the comprehensive weights. Then, an improved water yield property index (IWYPI) model is established, and the water yield zoning map of sandstone aquifers is acquired. Engineering practice shows that the evaluation accuracy of the water yield property index (IWYPI) model based on the CWM is as high as 93.75%, which is 18.75% and 12.5% higher than that of the water yield property index (WYPI) model based on the FDAHP and EWM, respectively. The research results propose a novel method for evaluating the water yield of coal seam roof aquifers and can provide scientific guidance for the prevention and control of water disasters in the no. 8 coal seam roof of the Donghuantuo Coal Mine.

1. Introduction

As the largest coal mining country in the world, China also has some of the most serious mine water disasters [1–3]. Especially with the large-scale development of deep resources, the prevention and control of water disasters remains a top priority and is complicated by many problems and challenges. Control and utilization of China's groundwater resources remain a major research topic in coal mine safety production and scientific mining research [4–6]. From 2000 to 2011, there were 1089 coal mine water accidents in China with a total death toll of 4329 [7]. In particular, North China-type coalfields in China not only suffer from the problem of water inrushes from coal seam floors but also face the threat of water catastrophes from coal seam roofs [8]. The sufficient and necessary conditions for the occurrence of water disasters in coal seam roofs are that mining and caving touch water-filled aquifers, and the corresponding areas have high water yields, i.e., the aquifer provides the material for the water inrush from the coal seam roof, and the water yield of the aquifer directly determines the amount and duration of the water inrush [9]. Therefore, how to effectively evaluate the water yield of coal seam roof aquifers and how to delineate the zones of coal seam roofs with high water yields based on reality has important guiding significance and practical value for the prevention and control of coal mine roof water disasters.

Studying the water yield properties of aquifers is essential for preventing and controlling water disasters in coal seam roofs, and several assessment methods have been developed in recent decades. Geophysical prospecting and pumping test

methods have been widely used and play an active role in the evaluation of aquifer water yields [10–17]. However, these two methods have problems, such as being the only method considered, a heavy workload, a high cost, and a limited control range, which limit their application [18]. Another important method is the analytic hierarchy process (AHP) water yield property index method [19], which uses geographic information systems (GIS) to fuse multisource geoscience information and to comprehensively reflect the results of water yield evaluations with various influencing factors and the differences and relationships among these factors. Compared with the geophysical prospecting method and the water pumping test method, the AHP has many potential advantages, but the weights of the factors influencing the water yield in this method are highly subjective as they are based on expert opinions; in addition, it is difficult to reach consistency in the judgement matrix in this method for more than four factors [20, 21]. Grey theory, BP neural networks, fuzzy clustering methods, and principal component analysis methods have been introduced for the evaluation of water yields, strengthening the evaluation of the water yield [22–25]. However, these methods have limitations in practical application, and they fail to address uncertain factors such as insufficient sample sizes, data information fusion, or subjective fuzzy evaluation in the evaluation process. For example, grey theory requires many water inrush examples and calculates the weight of each index according to the correlation coefficient between the index of each example and water inflow; however, when the amount of data is insufficient, the evaluation results are likely to deviate greatly [26]. The BP neural network model often results in overfitting, which usually leads to a local minimum and a slow convergence speed problem [27]. The fuzzy clustering method is theoretical and difficult to combine with actual mining areas [28]. However, principal component analysis effectively eliminates the influence of information superposition among evaluation indexes [29], but it compromises by making the evaluation index value fuzzy to reduce the dimensionality of the variables [30].

In summary, there are certain limitations to evaluate the water yield of an aquifer using any one method alone. Therefore, this paper proposes a water yield evaluation method based on the coupling of the fuzzy Delphi analytic hierarchy process (FDAHP) and entropy weight method (EWM) and applies it to evaluate the water yield of the sandstone aquifer in the roof of the Donghuantuo Coal Mine in a North China-type coalfield. The FDAHP and EWM are combined to determine the weight of each influencing factor. Considering the opinions of a group of decision-making experts, the problems of large errors from single-person evaluations and difficult consistency of the judgement matrix in the AHP are effectively avoided, and the characteristics of measured data are considered, thereby realizing the organic integration of subjective and objective weights and improving the accuracy and reliability of the evaluation results. Based on this, an improved water yield property index (IWYPI) model is established. The analysis results compared with engineering practice data are used to validate than the IWYPI model as an operational tool to evaluate the water yield of the no. 8 coal seam roof aquifer in the Donghuantuo Coal Mine. The obtained water yield zoning map of the sandstone aquifer provides a detailed scientific basis for ensuring safe coal mine production and roof water disaster prevention.

2. The Study Area

2.1. Physical Geography. The Donghuantuo Coal Mine is a typical North China Carboniferous-Permian coalfield with extremely complex hydrogeological conditions. During the construction period of the mine, the maximum water inflow reached 62.84 $m^3 \cdot min^{-1}$, and many water inrush accidents have occurred. At present, as the increase of the depth of coal mining, the threat of water hazards will continue to increase [31]. The Donghuantuo Mine is located in Tangshan City, Hebei Province (Figure 1). It is approximately 10 km east to Tangshan Station and 14 km south to Xugezhuang Station. The mine is within alluvial plain terrain; there are neither hills nor rivers in the mine area. The terrain is flat and high in the northeast and low in the southwest. The elevation of the terrain ranges from 2 to 23 m, and the topographic slope is 1.6. The climate of the mine area is continental: hot and rainy in summer and cold and windy in winter. The temperature ranges from 39.6 to -21°C with an average of 11.1°C. The average annual rainfall is 614.7 mm, and the average annual evaporation is 1321.1 mm. There is no surface water system in the mine area.

2.2. Geological Conditions. The Donghuantuo Coal Mine is in the northwestern Kaiping Coalfield. The strata of the Kaiping Coalfield are North China-type deposits. According to the strata exposed by boreholes, the study area contains Ordovician, Carboniferous, Permian and Quaternary strata. The coal-bearing strata in the mine are Carboniferous and Permian. The total thickness of the coal seams is 19.70 m, which includes the no. 8, no. 9, no. 11 and no. 12-1 main coal seams.

The mine is located on both sides of the Chezhoushan syncline, which is part of a coal-bearing structure in the western Kaiping Coalfield. Its main structural controls are those of the Neocathaysian system, and the structural lines are mostly NE-trending. The syncline is a large coal-bearing syncline with a long and narrow asymmetrical dip to the southwest. The strike of the syncline axis is approximately N60°E, and the synclinal axis slopes to the northwest.

Strata on both sides of the syncline vary greatly. The strata in the southeast wing are gentle with an inclination of approximately 20°, while the strata in the northwest wing are steep with an inclination of approximately 70°. The main structural form of the mine is the monoclinic structure in the southeastern wing of the Chezhoushan syncline. The fault structure is well developed in the mine, and the strike of the fault is mostly consistent with the direction of the syncline axis (Figure 2).

2.3. Hydrogeological Characteristics of the Mine. In this study, the main coal seam is the no. 8 coal seam, the direct water-filled aquifer is a Permian sandstone fractured aquifer, and the indirect water-filled aquifer is a Quaternary bottom gravel aquifer. There is a weak permeable aquifer between these two

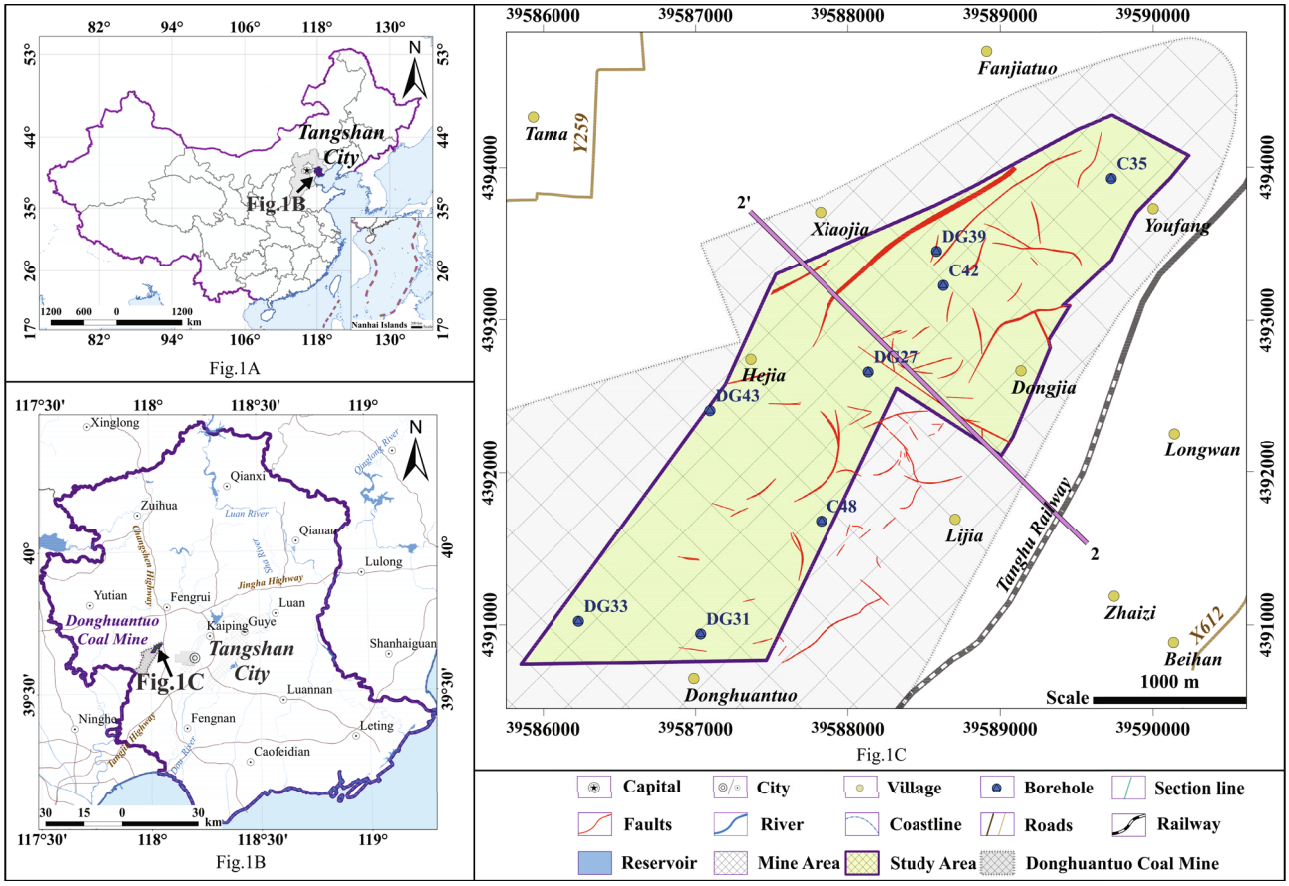

FIGURE 1: Map showing the location of the study area.

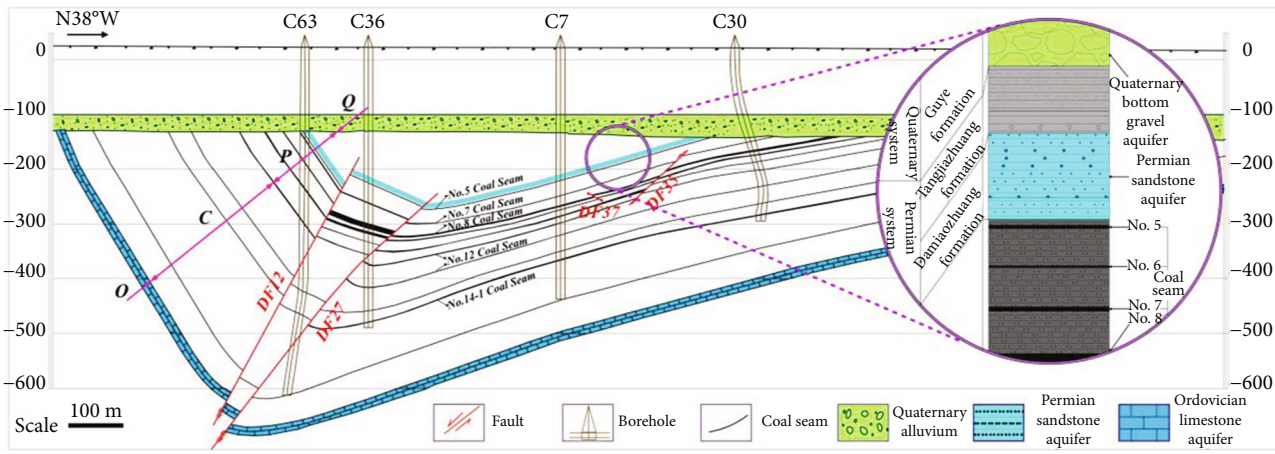

FIGURE 2: 2-2′ geological profile of the study area.

aquifers (Figure 2). The Permian sandstone fractured aquifer is the main threat to safely mining the no. 8 seam.

The Permian sandstone fractured aquifer is dominated by coarse sandstone and gravel-bearing giant sandstone with unequal grains and muddy siliceous cementation. This aquifer has extensive direct contact with the bottom gravel aquifer, and the gravel aquifer is the recharge source, so water is abundant and not easily drained. The specific capacity of boreholes is 0.016-1.806 $L \cdot s^{-1} \cdot m^{-1}$, and the permeability coefficient is 0.369-10.492 $m \cdot d^{-1}$.

The topographic difference between the outcrops in the two wings reveals that the northwest wing is a recharge area, and the southeast wing is an excretion area under natural conditions. The Permian sandstone fractured aquifer receives pore water from the bottom pebble beds of the Quaternary aquifer along the northwest wing. There has been a

fundamental change in the groundwater movement arising from the operation of the mine, with the underground mining area becoming a drainage area and the outcrop zones near the mining area of the north and south flanks becoming a recharge area. At present, groundwater drainage is achieved by mine pumping.

3. Data

3.1. Major Controlling Factors of the Aquifer Water Yield. A thorough analysis of the hydrogeological data of the mining area was performed to generate a thematic database of multivariate geological information to comprehensively reflect the water yield of the water-filled aquifer. This analysis comprised seven factors: the permeability coefficient, consumption of flushing fluid, aquifer thickness, ratio of brittle-plastic rock thickness, core recovery rate, fault point density, and fault scale index (Figures 3 and 4).

(1) The permeability coefficient is a constant representing the permeability of rock strata. Generally, the higher the permeability coefficient is, the more permeable the rock. The permeability of the Permian sandstone fractured aquifer in the study increased gradually from northeast to southwest in the range of 1.05-2.15 $m \cdot d^{-1}$

(2) The consumption of drilling fluid can reflect the permeability of the drilled rock. There is a certain degree of drilling fluid leakage when drilling through an aquifer. The larger the amount of leakage is, the better the development degree and connectivity of the voids in the strata. The flushing fluid consumption of the Permian sandstone fractured aquifer in the study area increased gradually from northeast to southwest within a range of 0.1-14.5 $m^3 \cdot h^{-1}$

(3) Aquifer thickness is the prerequisite for determining the water yield and the primary factor affecting the occurrence of groundwater. Generally, the thicker the aquifer is, the greater its water content. In the study area, the closer the Permian sandstone fractured aquifer was to the syncline axis, the thicker the aquifer was. The overall thickness increased gradually from northeast to southwest within a range of 140-230 m.

(4) The ratio of the brittle-to-plastic rock thickness can be used as an index to qualitatively judge the permeability of sandstone fractured aquifers. In the case of failure due to tectonic stress, the fracture characteristics reflected by lithologies with different mechanical properties are quite different. The stress release of brittle sandstone mainly occurs in the form of shear and tensile failures. Fractures and joints are relatively developed in the sandstone layer, which greatly enhances the permeability. Plastic clay rocks release their stress in the form of plastic deformation under a load action, which results in minimal changes to its permeability. Therefore, in general, the larger the ratio of brittle-to-plastic rock thickness is, the higher the permeability of the aquifer. The lithology of the Permian sandstone fractured aquifer in the study area is mainly medium and fine sandstone. Brittle rocks are much thicker than plastic rocks. Except in some individual sections, the ratio of the brittle-to-plastic rock thickness gradually decreased from northeast to southwest in the study area, ranging from 1.05-2.35.

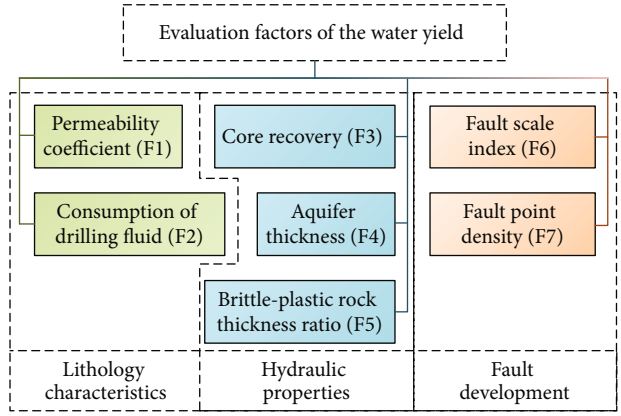

Figure 3: Major controlling factors of the water yield evaluation.

(5) Core recovery refers to the ratio of the core length to the drilling depth, which is expressed as a percentage. Core recovery is a rock quality index used to express the integrity of a rock mass. The lower the core rate is, the more fragmented the rock and the better its connectivity. The core recovery rate of the Permian sandstone fractured aquifer in the study area gradually decreased from northeast to southwest, ranging from 0.87 to 0.99.

(6) The density of fault points refers to the number of intersections and endpoints of faults in a unit area. Intersections and endpoints of faults form in space and along planes and have certain rules for development. The higher the fault point density is, the more developed the rock mass fissures and the higher the water content and water conductivity. There are many faults in the study area that are widely distributed. The geological profile shows that most of the faults cut the Permian sandstone fissure aquifer. The high density of fault points in the middle and southern parts of the study area indicates that the water yield of the Permian sandstone fractured aquifer is obviously affected by faults.

(7) The fault size index is the sum of the product of the fault throw and strike lengths of all faults in the unit area, as shown by

$$F = \frac{\sum_{i=1}^{n} L_i H_i}{S}, \quad (1)$$

where F is the fault size index, H_i is the fault throw of the i^{th} fault (m), L_i is the strike length of the i^{th} fault

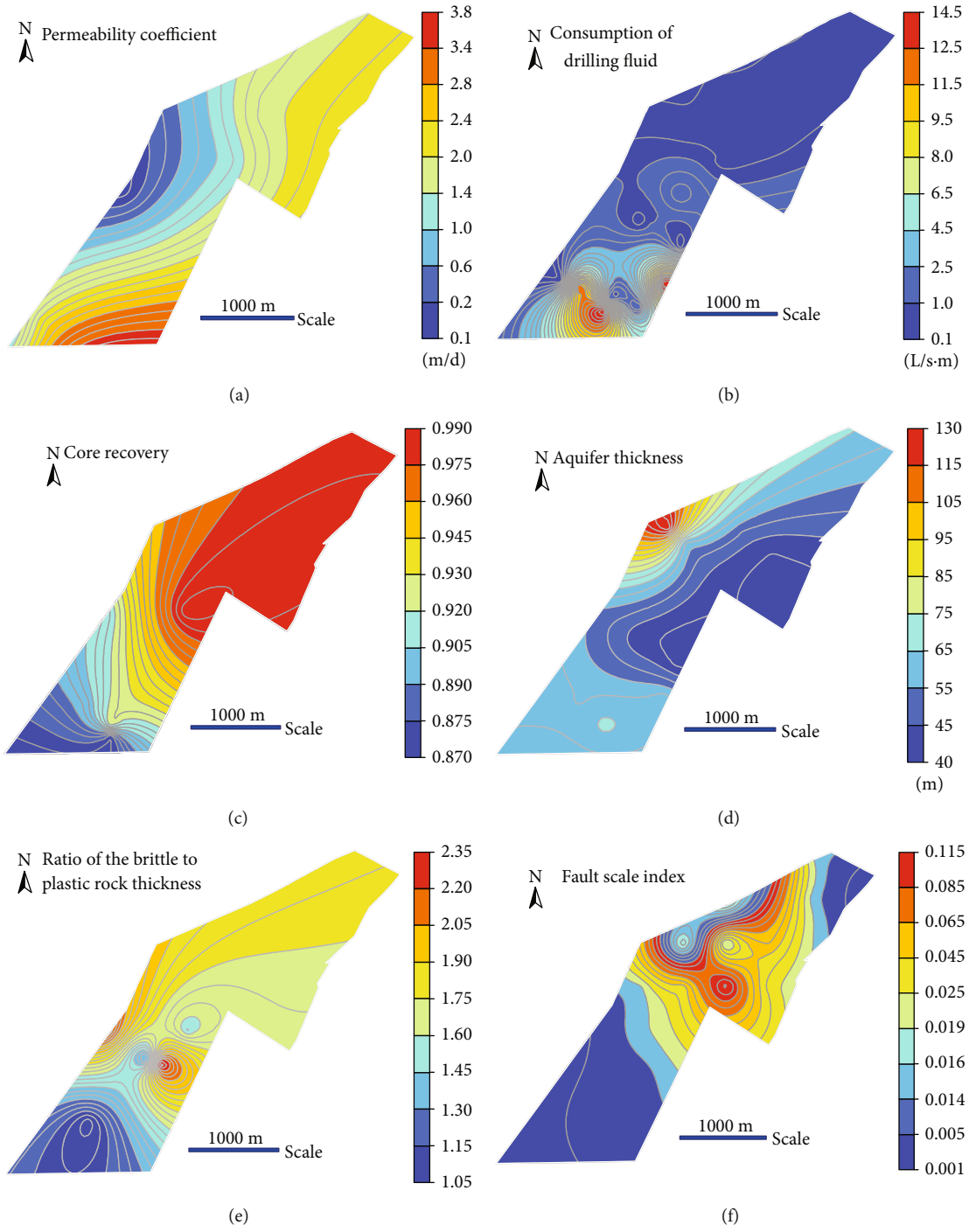

Figure 4: Continued.

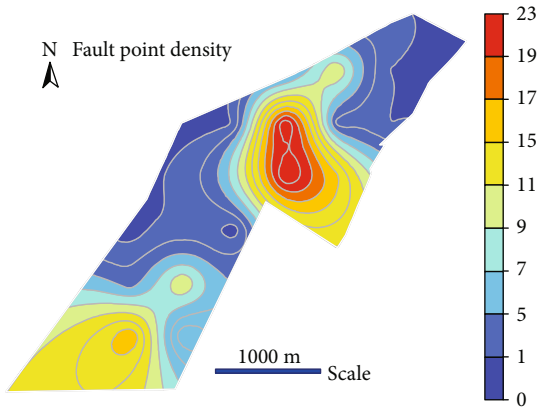

(g)

Figure 4: Thematic map of multiple geological factors for the water-filled aquifer in the no. 8 coal seam roof.

in the unit area (m), N is the number of faults within the unit area, and S is the unit area (m^2).

The fault size index comprehensively reflects the size and development of faults. The larger the fault size index is, the larger the groundwater recharge scope and occurrence space and the higher the water yield of the faults. The large-scale index of faults in the central and northern parts of the study area indicates that the area is disturbed by faults, and faults may serve as water-filling sources or conduits to increase the possibility of roof water inrushes.

3.2. Data Normalization. Taken individually, components of multivariate geological information provide only a limited reflection of the aquifer water yield, and data integration is necessary to comprehensively reflect the aquifer water yield. The physical quantities of aquifers represented by multivariate geological information are different. To achieve data integration, the limitations of different physical dimensions must first be eliminated. Normalization of data is a feasible way to achieve this, and Equations (2) and (3) were used to normalize the factors from the established multivariate geological information database, which were positively and negatively correlated with the water yield, respectively.

$$y_i = \frac{x_i - x_{\min}}{x_{\max} - x_{\min}}, \tag{2}$$

$$y_i' = \frac{x_{\max} - x_i}{x_{\max} - x_{\min}}. \tag{3}$$

y_i and y_i' are the normalized value for positive and negative factor respectively, while $x_{\max}$ and $x_{\min}$ are the maximum and minimum of the original data, respectively. In this paper, the evaluation factors were normalized by Equation (2), with the exception of the core recovery factor, which was calculated by Equation (3).

4. Methods

4.1. Procedures. To acquire a relatively reasonable and accurate evaluation of the water yield of the coal roof aquifer, the comprehensive weight should be determined by considering the fuzziness of the comprehensive evaluation process, the decision-making experience of the expert group, and the differential information of the evaluation factor.

Based on the scientific quantification of multiple factors, the synthesized evaluation applies comprehensive coupling of the FDAHP and EWM, as shown in Figure 5.

4.2. Determination of the Factor Weights

4.2.1. Subjective Weights by the FDAHP. The FDAHP is a fuzzy group decision-making method that integrates fuzzy mathematics appraisal and the AHP and the Delphi group decision-making method [32, 33]. The relative importance matrix (Table 1) for all determined factors according to each expert's judgement value by the Saaty scale method is essential and the basis of generating a pairwise comparison matrix.

According to expert opinions, F1, F2,…, F7 are the evaluation factors, while a_{ij} is defined as the relative importance comparison judgement value for a pair of factors and is obtained by the F_i value divided by the F_j value. Therefore, ten 7×7 pairwise comparison judgement matrices for each expert were generated.

$$A = \begin{bmatrix} 1 & a_{12} & \cdots & a_{17} \\ \frac{1}{a_{12}} & 1 & \cdots & a_{27} \\ \vdots & \vdots & \ddots & \vdots \\ \frac{1}{a_{17}} & \frac{1}{a_{27}} & \cdots & 1 \end{bmatrix}. \tag{4}$$

Then, a group of fuzzy pairwise comparison matrices was established by making use of the triangular fuzzy number b_{ij}, which was calculated using Equation (5) and consisted of pessimistic, moderate, and optimistic comparison judgements of the evaluation factor according to the opinions of ten experts.

$$b_{ij} = \left(\alpha_{ij}, \beta_{ij}, \gamma_{ij}\right). \tag{5}$$

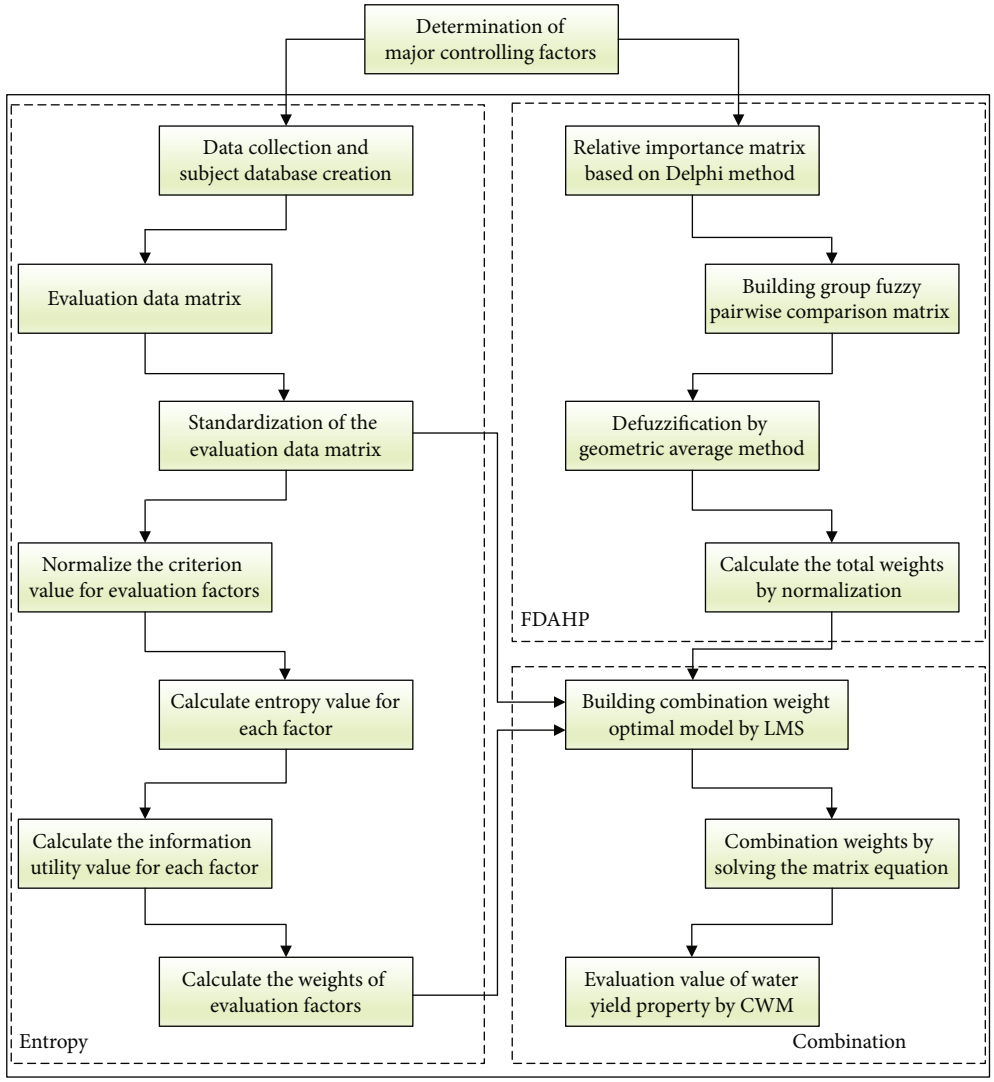

Figure 5: Flowchart of the methodology.

Table 1: Relative importance matrix of evaluation factors.

Factor	Expert 1 (E1)	Expert 2 (E2)	Expert 3 (E3)	Expert 4 (E4)	Expert 5 (E5)	Expert 6 (E6)	Expert 7 (E7)	Expert 8 (E8)	Expert 9 (E9)	Expert10 (E10)
Permeability coefficient (F1)	9	9	9	8	9	8	9	9	9	9
Consumption of drilling fluid (F2)	4	4	5	4	5	4	4	4	4	4
Core recovery (F3)	3	4	3	5	3	3	3	4	5	3
Aquifer thickness (F4)	8	8	7	8	7	9	7	8	7	7
Brittle-plastic rock thickness ratio (F4)	3	3	3	3	3	3	4	4	3	3
Fault scale index (F5)	4	4	4	4	5	4	4	3	4	5
Fault point density (F6)	3	2	3	2	2	3	3	2	2	3

$\alpha_{ij} \le \beta_{ij} \le \gamma_{ij}$, and they are obtained separately by Equations (6), (7), and (8). Furthermore, the established group fuzzy pairwise comparison matrix in this paper is shown in Table 2.

$$\alpha_{ij} = \min\left(b_{ijk}\right), \quad k = 1, 2, \cdots, p, \tag{6}$$

$$\beta_{ij} = \left(\prod_{k=1}^{m}\left(b_{ijk}\right)\right)^{1/m}, \quad k = 1, 2, \cdots, p, \tag{7}$$

$$\gamma_{ij} = \max\left(b_{ijk}\right), \quad k = 1, 2, \cdots, p. \tag{8}$$

Table 2: Group fuzzy pairwise comparison matrix.

	F1	F2	F3	F4	F5	F6	F7
F1	(1.00, 1.00, 1.00)	(1.80, 2.15, 2.25)	(1.80, 2.56, 3.00)	(1.13, 1.27, 1.50)	(2.25, 2.83, 3.00)	(1.80, 2.21, 3.00)	(3.00, 3.25, 4.50)
F2	(0.44, 0.46, 0.56)	(1.00, 1.00, 1.00)	(0.80, 1.19, 1.67)	(0.50, 0.59, 0.71)	(1.00, 1.32, 1.67)	(0.80, 1.03, 1.33)	(1.33, 1.51, 2.50)
F3	(0.33, 0.39, 0.56)	(0.60, 0.84, 1.25)	(1.00, 1.00, 1.00)	(0.38, 0.50, 0.83)	(0.75, 1.11, 1.67)	(0.60, 0.87, 1.33)	(1.00, 1.27, 2.50)
F4	(0.67, 0.78, 0.89)	(1.40, 1.69, 2.00)	(1.20, 2.01, 2.67)	(1.00, 1.00, 1.00)	(1.75, 2.26, 2.67)	(1.40, 1.77, 2.67)	(2.00, 2.59, 3.50)
F5	(0.33, 0.35, 0.44)	(0.60, 0.76, 1.00)	(0.60, 0.90, 1.33)	(0.38, 0.44, 0.57)	(1.00, 1.00, 1.00)	(0.60, 0.76, 1.00)	(1.00, 1.12, 1.50)
F6	(0.33, 0.45, 0.56)	(0.75, 0.97, 1.25)	(0.75, 1.15, 1.67)	(0.38, 0.57, 0.71)	(1.00, 1.32, 1.67)	(1.00, 1.00, 1.00)	(1.00, 1.47, 2.50)
F7	(0.22, 0.31, 0.33)	(0.40, 0.66, 0.75)	(0.40, 0.79, 1.00)	(0.29, 0.39, 0.50)	(0.67, 0.90, 1.00)	(0.40, 0.68, 1.00)	(1.00, 1.00, 1.00)

In the following defuzzification process, the geometric average method is applied to acquire the relative fuzzy weights for each factor. The group fuzzy weight vector and the fuzzy weights vector are determined by calculating Equations (9) and (10) successively.

$$r_i = (a_{i1} \otimes a_{i2} \otimes \cdots \otimes a_{in})^{1/n}, \tag{9}$$

$$w_i = r_i \otimes (r_1 \otimes r_2 \otimes \cdots \otimes r_n)^{-1}. \tag{10}$$

The two triangular fuzzy numbers $[a_1, a_2, a_3]$ and $[b_1, b_2, b_3]$ are calculated using

$$a \oplus b = [a_1 + b_1, a_2 + b_2, a_3 + b_3], \tag{11}$$

$$a \otimes b = [a_1 \times b_1, a_2 \times b_2, a_3 \times b_3], \tag{12}$$

$$a^{-1} = \left[a3^{-1}, a2^{-1}, a1^{-1}\right]. \tag{13}$$

Finally, the weights for each evaluation factor were obtained by the normalization of the fuzzy weight vector (w_i^L, w_i^M, w_i^N) by calculating Equation (14), and the results are shown in Table 3.

$$Ui = \frac{\left(w_i^L \times w_i^M \times w_i^N\right)^{1/3}}{\sum_{i=1}^{m}\left(w_i^L \times w_i^M \times w_i^N\right)^{1/3}}. \tag{14}$$

4.2.2. Objective Weights by the EWM. As a quantitative objective weighting method, the EWM can determine the factor weights according to the degree of variation in the major controlling factors by using information entropy to measure the uncertainty and heterogeneity of the factor value distribution.

For a certain factor value, the uneven distribution usually shows a significant difference in heterogeneity and manifests as a higher entropy but a lower entropy weight. Therefore, the existing objective criteria for weighting could avoid the influence of subjective factors as much as possible.

To obtain information entropy for each evaluation factor by the EWM [34], the standardized matrix Y_{ij} was established and expressed as Equation (15), which consisted of standardized data with 5787 evaluation units from united spatial thematic data of 7 evaluation factors calculated by Equations (2) and (3). Thus, $i = 1, 2, 3, \cdots, 5787$, and $j = 1, 2, 3, \cdots, 7$ in this paper.

Table 3: Calculated group fuzzy weights and total weights by the FDAHP.

Evaluation factors	Group fuzzy weights	Total weights
F1	(0.1796, 0.2663, 0.3866)	0.2647
F2	(0.0824, 0.1237, 0.1971)	0.1263
F3	(0.0644, 0.1041, 0.1934)	0.1092
F4	(0.1333, 0.2104, 0.3236)	0.2088
F5	(0.0624, 0.0930, 0.1486)	0.0953
F6	(0.0715, 0.1205, 0.1953)	0.1191
F7	(0.0449, 0.0820, 0.1216)	0.0766

$$Y = \left[Y_{ij}\right] = \begin{bmatrix} y_{11} & y_{12} & \cdots & y_{17} \\ y_{21} & y_{22} & \cdots & y_{27} \\ \vdots & \vdots & \ddots & \vdots \\ y_{57871} & y_{57872} & \cdots & y_{57877} \end{bmatrix}. \tag{15}$$

Then, Y_{ij} was normalized to calculate the projected outcome P_{ij} of the j^{th} factor by

$$P_{ij} = \frac{Y_{ij}}{\sum_{i=1}^{m} Y_{ij}}. \tag{16}$$

Then, the information entropy E_j could be defined as Equation (17), as shown in Table 4.

$$E_j = -(\ln m)^{-1} \sum_{i=1}^{m} P_{ij} \ln P_{ij}. \tag{17}$$

The diversification degree of information based on the j^{th} factor value d_j could be expressed as $d_j = 1 - E_j$, and the entropy weights of each factor were calculated by following Equation (18) and are shown in Table 4.

$$V_j = \frac{d_j}{\sum_{j=1}^{n} d_j}. \tag{18}$$

4.2.3. Total Weights by the CWM. Whereas the a priori weighting method FDAHP can provide subjective weights by

considering the fuzziness of the evaluation process by group decision-making, and the EWM can determine the objective assessment with good stability upon attribute preference, the combination weight model (CWM) based on the optimization method is proposed in this paper. In situations that consider both the experience of a group of experts and the objective datum situation, the CWM can provide practical and reasonable weights.

The judgement basis of the CWM can be expressed as follows: the total deviation between the FDAHP calculations and the EWM result should be as small as possible. Therefore, the optimization model that applies the least square method to combine the subjective weight of a group of experts u_j with the objective entropy weight v_j is established as [35]

$$\min\ D(w) = \sum_{i=1}^{m}\sum_{j=1}^{n}\left\{\left[\left(u_j - w_j\right)Y_{ij}\right]^2 + \left[\left(v_j - w_j\right)Y_{ij}\right]^2\right\}, \tag{19}$$

$$\text{s.t.}\quad \sum_{j=1}^{n} w_j = 1, \tag{20}$$

$$w_j > 0. \tag{21}$$

Furthermore, the CWM optimization model can be expressed as Equation (22) by the Lagrangian transformation.

$$\begin{bmatrix} A & e \\ e^T & 0 \end{bmatrix} \times \begin{bmatrix} w_j \\ \lambda \end{bmatrix} = \begin{bmatrix} B \\ 1 \end{bmatrix}. \tag{22}$$

The diagonal matrix A and the vector matrices e, W, and B are defined as Equations (23) to (26), respectively.

$$A = \text{diag}\left[\sum_{i=1}^{m} Y_{i1}^2, \sum_{i=1}^{m} Y_{i2}^2, \cdots, \sum_{i=1}^{m} Y_{\text{in}}^2\right], \tag{23}$$

$$e = [1, 1, \cdots, 1]^T, \tag{24}$$

$$w_j = [w_1, w_2, \cdots, w_n]^T, \tag{25}$$

$$B = \left[\sum_{i=1}^{m}\frac{1}{2}(u_1 + v_1)Y_{i1}^2, \sum_{i=1}^{m}\frac{1}{2}(u_2 + v_2)Y_{i2}^2, \cdots, \sum_{i=1}^{m}\frac{1}{2}(u_n + v_n)Y_{\text{in}}^2\right]^T. \tag{26}$$

In this paper, the 7×7 matrix A was established by calculating the square sum of each factor, as shown by Equation (27), and the subjective weight u_j in Equation (26) was obtained from the FDAHP weighting process, while the objective weight v_j was acquired based on the measured information entropy of controlling factors by the EWM method.

$$A = \begin{bmatrix} 1661.2474 & 0 & 0 & 0 & 0 & 0 & 0 \\ 0 & 755.0315 & 0 & 0 & 0 & 0 & 0 \\ 0 & 0 & 1585.8033 & 0 & 0 & 0 & 0 \\ 0 & 0 & 0 & 547.9346 & 0 & 0 & 0 \\ 0 & 0 & 0 & 0 & 1310.3613 & 0 & 0 \\ 0 & 0 & 0 & 0 & 0 & 445.8467 & 0 \\ 0 & 0 & 0 & 0 & 0 & 0 & 1097.3887 \end{bmatrix}. \tag{27}$$

Finally, the CWM weights were acquired by calculating Equation (28), and the combination weight 5787 coupling of the subjective weight u_j and objective entropy weight v_j is shown in Table 5.

$$W_j = A^{-1} \times \left[B + \frac{1 - e^T A^{-1} B}{e^T A^{-1} e} \times e\right]. \tag{28}$$

4.3. Evaluation of the IWYPI Model. The distribution of the aquifer water yield is controlled by a combination of factors; therefore, the comprehensive analysis of multisource information is considered to be the best method to evaluate the water yield of coal roof aquifers [36–38]. Based on the statistical values of 7 influencing factors of 36 boreholes in the northern no. 2 mining area and central mining area of the Donghuantuo Coal Mine, this paper first standardizes these factors and then applies the spatial information processing and analysis function of GIS to integrate the information of the 7 factors affecting the aquifer water yield.

On this basis, combined with the CWM composed of the FDAHP and EWM, an IWYPI model is established by adding linear weights to quantitatively describe the comprehensive influence of aquifer lithology, aquifer hydraulic properties, and fault characteristics of different weight combinations on the aquifer water yield. The calculation formula is shown by

$$\text{WI} = \sum_{j=1}^{n} W_j * f_j(x, y). \tag{29}$$

Table 4: The entropy and entropy weights of evaluation factors.

Factor	F1	F2	F3	F4	F5	F6	F7
Entropy E	0.9841	0.9446	0.9715	0.9749	0.9788	0.9118	0.9752
Entropy weight V	0.0615	0.2137	0.1101	0.0967	0.0819	0.3405	0.0956

Table 5: The calculated weights of evaluation factors by the FDAHP, EWM, and CWM.

Factor	F1	F2	F3	F4	F5	F6	F7
FDAHP weight U	0.2647	0.1263	0.1092	0.2088	0.0953	0.1191	0.0766
Entropy weight V	0.0615	0.2137	0.1101	0.0967	0.0819	0.3405	0.0956
Combination weight W	0.1631	0.1701	0.1096	0.1527	0.0886	0.2298	0.0861

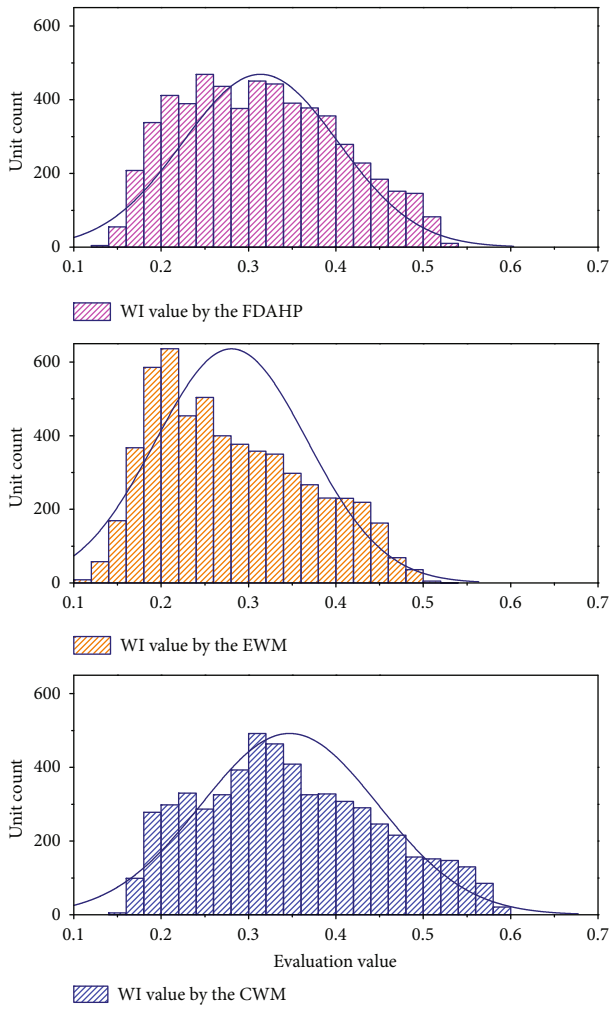

Figure 6: Frequency histogram of the WI.

where WI is the aquifer water yield property index; j is the factor number; n is the number of factors, which is 7 in this paper; W_j is the weight value of the j^{th} factor; $f_j(x, y)$ is the standard value of the j^{th} factor; and (x, y) are geographic coordinates.

The IWYPI model in this paper is established according to Equation (29) and shown as Equation (30). Correspondingly, the water yield property index (WYPI) model weighted by the FDAHP and EWM can also be calculated by Equation (29).

$$\begin{aligned} \mathrm{WI} = {} & 0.1631 * f_1(x, y) + 0.1701 * f_2(x, y) \\ & + 0.1096 * f_3(x, y) + 0.1527 * f_4(x, y) \\ & + 0.0086 * f_5(x, y) + 0.2298 * f_6(x, y) \\ & + 0.0861 * f_7(x, y). \end{aligned} \tag{30}$$

5. Results and Discussion

5.1. Results. According to the IWYPI and WYPI models, which have different weighting methods, the water yield zoning maps of the roof sandstone aquifer of the no. 8 coal seam are constructed by using GIS spatial superposition and reclassification functions, and a frequency histogram of WI values calculated by the three methods is acquired (Figure 6). As shown in Figures 7–9, there are differences in the evaluated WI values calculated from the different methods, with a larger value indicating a higher water yield. The WI values calculated by the FDAHP are 0.1549~0.5941, the WI values calculated by the EWM are 0.1131~0.5216, and the WI values calculated by the CWM are 0.1357~0.5271. Furthermore, the corresponding classification thresholds of WI values for four levels are determined by the natural break algorithm embedded in the GIS classification method. Therefore, the least square sum of the WI value and corresponding mean value are obtained by iterative grouping for determining thresholds. According to the classification threshold (Table 6), the water yield is divided into the following zones: poor, medium, rich, and richer; the distribution of partitions for each evaluation result is shown in Figures 7–9.

As shown in Figures 7–9, the overall trends of the results of the evaluation of the aquifer water yield by the three methods are consistent. The results are also cross-verified, which indicates that the water yield of the sandstone aquifer in the no. 8 coal seam roof in the Donghuantuo Mine ranges from poor to richer, among which the rich and richer zones are mainly distributed in the southern and middle regions, the medium zones are mainly distributed in the northern and middle regions, and the poor zones are mainly distributed in the northeast and central and western regions. As shown in Figures 4(a)–4(g), the difference in the water yield in the study area is mainly related to the aquifer permeability

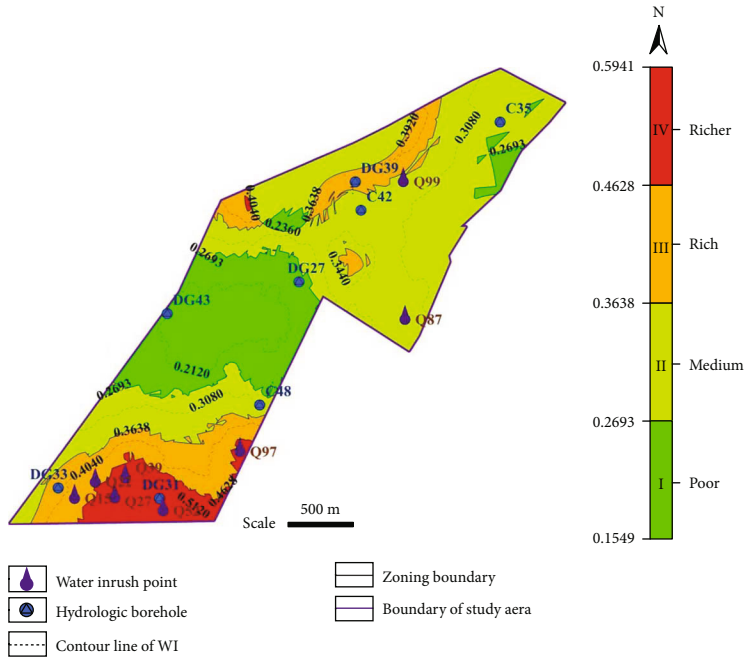

Figure 7: Water yield zoning map based on the WYPI model weighted by the FDAHP.

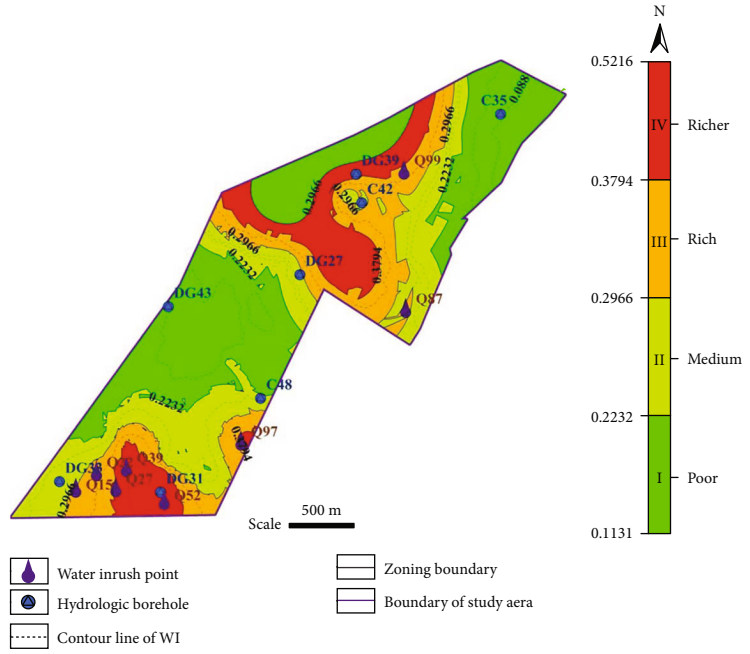

Figure 8: Water yield zoning map based on the WYPI model weighted by the EWM.

coefficient, thickness, and fault development, and the water yield in the zones with high values of these factors is relatively high. For example, the permeability coefficient and consumption of drilling fluid in the southern part of the study area are high, so the evaluation results of the three methods in the south indicate zones with rich-richer water yields. The fault scale index and fault point density in the middle of the study area are high, and the evaluation results of the middle of the study area by the three methods indicate medium-richer water yields. In contrast, except for the ratio of the brittle-to-plastic rock thickness, the water yield in areas with low index values is relatively poor, such as in the central and western regions of the study area, and the evaluation results of the three methods indicate zones with poor water yields.

5.2. Engineering Practice. According to the Regulations for Coal Water Prevention and Control in China [39], the theoretical evaluation of the aquifer water yield is based on a unit of water inflow (represented by q); however, the pumping test

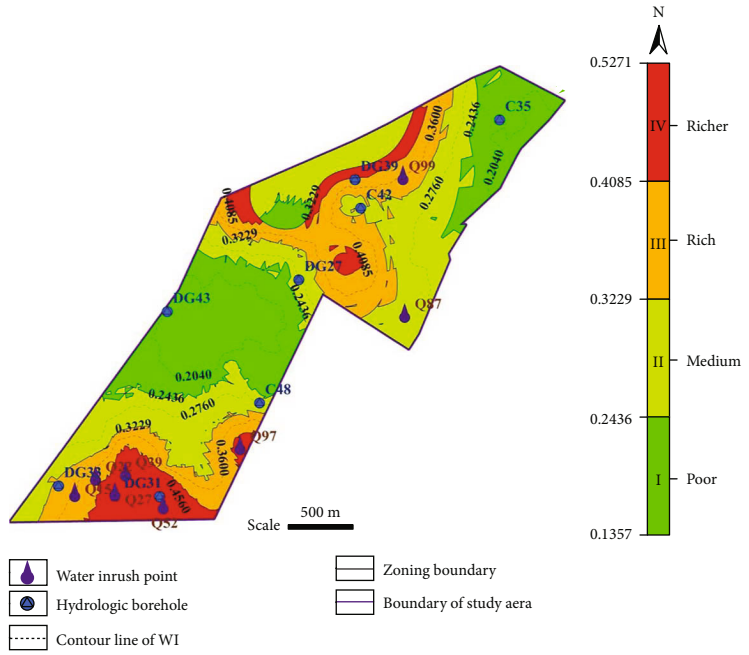

Figure 9: Water yield zoning map based on the IWYPI model weighted by the CWM.

Table 6: Classification thresholds of WI values by the FDAHP, EWM, and CWM.

Partition code	Water yield zone	WI value by the FDAHP	WI value by the EWM	WI value by the CWM
Zone I	Poor	0.1549-0.2693	0.1131-0.2232	0.1357-0.2436
Zone II	Medium	0.2694-0.3638	0.2233-0.2966	0.2437-0.3229
Zone III	Rich	0.3639-0.4628	0.2967-0.3794	0.3230-0.4085
Zone IV	Richer	Greater than 0.4628	Greater than 0.3794	Greater than 0.4085

Table 7: Specified and revised classification standard for the water yield.

	Specified level	Specified q ($L{\cdot}s^{-1}{\cdot}m^{-1}$)		Partition code	Revised level	Revised q ($L{\cdot}s^{-1}{\cdot}m^{-1}$)	Q ($m^3{\cdot}min^{-1}$)
Specified classification standard	Weak	$q \le 0.1$	Revised classification standard	Zone I	Poor	$q \le 0.1$	$Q < 0.2$
	Medium	$0.1 < q \le 1.0$		Zone II	Medium	$0.1 < q \le 1.0$	$0.2 \le q < 1.0$
	Rich	$1.0 < q \le 5.0$		Zone III	Rich	$1.0 < q \le 1.5$	$1.0 \le q < 2.0$
				Zone IV	Richer	$q > 1.5$	$q \ge 2.0$
	Extremely rich	$q > 5.0$		—	—	—	—

boreholes in the coalfield are generally limited in number and unevenly distributed. It is difficult to scientifically and reasonably divide the water yield of the aquifer by the q value. Therefore, the FDAHP, EWM, and CWM methods were used to establish a multisource geoscience information fusion WYPI model and an IWYPI model, which provide the more comprehensive scientific basis for the evaluation of the aquifer water yield.

Validation is the key to verifying results [40, 41]. The unit water inflow of the pumping test boreholes (represented by q) can directly indicate the water yield of aquifers. When data on the unit water inflow of the borehole are lacking, the inflow of the water inrush point (represented by Q) can also be used as the direct basis of the aquifer water yield. Therefore, the q and Q values are reliable bases to verify the evaluation results of different methods.

The q value can be divided into four grades (Table 7), poor, medium, rich, and extremely rich, according to the Regulations for Coal Water Prevention and Control in China. According to Table 7, the q values of 8 boreholes in the sandstone aquifer of the no. 8 coal roof in the study area are analysed. Among these q values, the boreholes with a medium water yield account for 50%, and the boreholes with both poor and rich water yields account for 25%; the maximum q value of the boreholes is 1.806 $L{\cdot}s^{-1}{\cdot}m^{-1}$, which is a rich water yield, and no boreholes with extremely rich water yields are found. To make the evaluation results of water yield zoning more convenient for conducting mine water

Table 8: Validation between the evaluation results and actual results.

Type and no. of verification case		Name	Measured q ($L{\cdot}s^{-1}{\cdot}m^{-1}$)	Measured Q ($m^3{\cdot}min^{-1}$)	Actual Judgment	WYPI result by the FDAHP		WYPI result by the EWM		IWYPI result by the CWM	
Hydrologic borehole	1	C35	0.086	—	I	II	Disagree	I	Agree	I	Agree
	2	DG39	0.110	—	II	III	Disagree	IV	Disagree	III	Disagree
	3	C42	0.143	—	II	II	Agree	II	Agree	II	Agree
	4	DG27	0.183	—	II	I	Disagree	II	Agree	II	Agree
	5	DG43	0.018	—	I	I	Agree	I	Agree	I	Agree
	6	C48	0.610	—	II	II	Agree	II	Agree	II	Agree
	7	DG33	1.222	—	III	III	Agree	II	Disagree	III	Agree
	8	DG31	1.806	—	IV	IV	Agree	IV	Agree	IV	Agree
Water inrush point	9	Q99	—	1.80	III	II	Disagree	III	Agree	III	Agree
	10	Q87	—	0.90	II	II	Agree	III	Disagree	II	Agree
	11	Q97	—	2.00	IV	IV	Agree	IV	Agree	IV	Agree
	12	Q15	—	1.02	III	III	Agree	III	Agree	III	Agree
	13	Q22	—	1.00	III	III	Agree	III	Agree	III	Agree
	14	Q39	—	4.57	IV	IV	Agree	IV	Agree	IV	Agree
	15	Q52	—	4.00	IV	IV	Agree	IV	Agree	IV	Agree
	16	Q27	—	3.19	IV	IV	Agree	IV	Agree	IV	Agree

prevention and control work in the Donghuantuo Coal Mine, the rich water yields can be further subdivided, that is, the rich water yield ($1{\sim}5\ L{\cdot}s^{-1}{\cdot}m^{-1}$) in the "Regulations" can be further divided into rich ($1{\sim}1.5\ L{\cdot}s^{-1}{\cdot}m^{-1}$) and richer ($1.5{\sim}2\ L{\cdot}s^{-1}{\cdot}m^{-1}$) water yields, as shown in Table 7. The revised classification standard of the water yield is suitable for the Donghuantuo Coal Mine. In the actual coal mining project of the Donghuantuo Coal Mine, the Q value is used to classify the water yield by taking the maximum inflow of each water inrush point in the Donghuantuo Mine in the last 10 years as the classification basis (Table 7).

Therefore, to verify the accuracy of the evaluation results of the FDAHP, EWM, and CWM, the evaluation results are compared with the actual engineering data, and a verification test is carried out. A total of 16 engineering test samples were collected, including 8 water inrush points and the q values of 8 boreholes in the Permian sandstone aquifer, and the evaluation results were tested. The evaluation results of these three methods and the actual results of 18 test samples are shown in Table 8. The results show that the coincidence degrees of the evaluation results of the FDAHP, EWM, and CWM with the actual results are 75%, 81.25%, and 93.75%, respectively; that is, the accuracy of the CWM is the highest.

6. Discussion

Through the verification of the evaluation results of the three methods, the evaluation ability of the CWM is the best, and its correctness percentage is as high as 93.75%, which is 18.75% and 12.5% higher than that of the FDAHP and EWM, respectively. The results of the FDAHP, EWM, and CWM are compared to determine the differences among the three evaluation methods. There are differences in the proportional area of each water yield grade evaluated by different methods (Figure 10).

According to the proportional area of each water yield grade from small to large, the water yields evaluated by the FDAHP and CWM are IV, III, I, and II, and the water yield grades evaluated by the EWM are IV, III, II, and I. This shows that the proportional area evaluated by the EWM for the poor water yield is relatively large, while for rich and richer water yields, which more easily cause water disasters in coal seam roofs, the proportional areas calculated by the FDAHP, EWM, and CWM are 24.19%, 33.95%, and 33.56%, respectively; this indicates that the proportional areas evaluated by the FDAHP for the rich and richer water yield areas are relatively small. Two main reasons account for these differences: (1) the FDAHP focuses on the influence of hydraulic properties of aquifers on the water yield and underestimates the influence of fault development characteristics on the water yield. For example, water inrush point Q99 is located in the fault development area and is affected by normal fault DF25 with a fault distance of 9 m. The aquifer fissure at this point is developed, with the water inflow reaching $1.8\ m^3{\cdot}min^{-1}$ and the aquifer having a rich water yield. However, the FDAHP classifies it as a medium water yield, which is inconsistent with the actual situation. (2) The EWM overemphasizes the difference in fault development characteristics in the study area but weakens the important influence of the aquifer permeability coefficient and thickness on the water yields. For example, the q value of the DG33 borehole is $1.22\ L{\cdot}s^{-1}{\cdot}m^{-1}$, and the sandstone aquifer where it is located is 60 m thick, with a permeability coefficient of $2.2\ m{\cdot}d^{-1}$, which is a rich water yield. It is unreasonable to characterize it as a medium water yield based on the EWM. Thus, the CWM takes into account both the recommendations of the experts and the internal relations among various

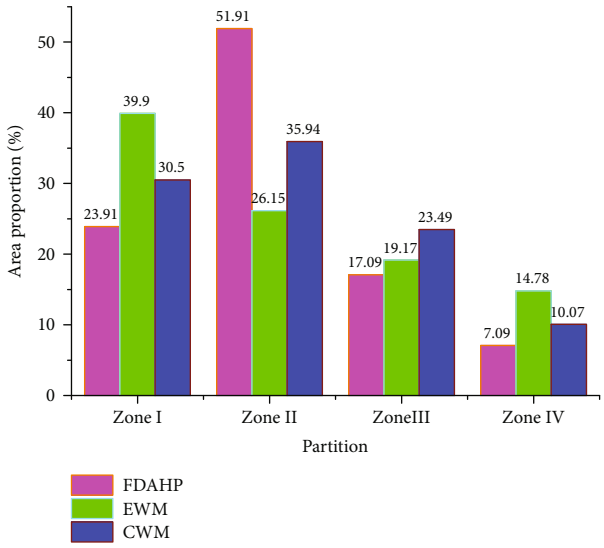

Figure 10: The proportional area of partition types for different results.

factors of the water yield; the CWM effectively reflects the joint control of the aquifer lithology, hydraulic characteristics, and fault factors on the water yield of the sandstone aquifer of the no. 8 coal seam roof in the study area, making the evaluation results more closely follow reality; moreover, the CWM can analyse the water yield characteristics of the coal seam roof more reasonably and accurately.

7. Conclusions

(1) Aquifers with rich and richer water yields provide the material source for water disasters in coal seam roofs, and they are also a prominent problem threatening the safe production of coal seams. It is necessary but challenging to evaluate the water yield of coal roof aquifers. The IWYPI model of coal roof aquifers is proposed and applied to evaluate the water yield of the sandstone aquifer in the no. 8 coal seam roof in the Donghuantuo Coal Mine. The factors that affect the water yield are the permeability coefficient, consumption of drilling fluid, core recovery, aquifer thickness, brittle-plastic rock thickness ratio, fault scale index, and fault point density. The IWYPI model established by the CWM takes into account the internal relations between the opinions of experts and various factors influencing the water yield; this model effectively reflects the common control of aquifer lithology, hydraulic characteristics, and fault factors on the aquifer water yield and overcomes the problem that there are generally limited amounts of water inflow data for boreholes in mines

(2) Engineering practice shows that the accuracy of the IWYPI model based on the CWM is as high as 93.75%, which is 18.75% and 12.5% higher than that of the WYPI model based on the FDAHP and EWM, respectively. The evaluation results show that the zones with rich and richer water yields are mainly distributed in the southern and middle regions, the zones with medium water yields are mainly distributed in the northern and middle regions, and the zones with poor water yields are mainly distributed in the northeast, central, and western regions. The IWYPI model provides favourable technical support for the prevention and control of water disasters in coal seam roofs and has important practical significance for ensuring safe coal mine production.

Data Availability

The data that support the findings of this study are available from the corresponding author upon reasonable request.

Conflicts of Interest

The authors declare no conflict of interest.

Acknowledgments

This study is financially supported by the National Natural Science Foundation of China (Granted No. 41702264), National Key Research and Development Program of China (2016YFC0402803-02), and China Three Gorges Group Co., Ltd. Project (0799217).

References

[1] S. N. Dong, L. W. Zheng, S. L. Tang, and P. Z. Shi, "A scientometric analysis of trends in coal mine water inrush prevention and control for the period 2000–2019," *Mine Water and the Environment*, vol. 39, no. 1, pp. 3–12, 2020.

[2] W. Qiang, L. Yuanzhang, and Y. Liu, "Using the vulnerable index method to assess the likelihood of a water inrush through the floor of a multi-seam coal mine in China," *Mine Water and the Environment*, vol. 30, no. 1, pp. 54–60, 2011.

[3] B. Li, X. Q. Wang, Z. J. Liu, and T. Li, "Study on multi-field catastrophe evolution laws of water inrush from concealed karst cave in roadway excavation: a case of Jiyuan coal mine," *Geomatics, Natural Hazards and Risk*, vol. 12, no. 1, pp. 222–243, 2021.

[4] H. F. Duan and L. J. Zhao, "New evaluation and prediction method to determine the risk of water inrush from mining coal seam floor," *Environmental Earth Sciences*, vol. 80, no. 1, 2021.

[5] Y. Zeng, Q. Wu, S. Liu, Y. Zhai, H. Lian, and W. Zhang, "Evaluation of a coal seam roof water inrush: case study in the Wangjialing coal mine, China," *Mine Water and the Environment*, vol. 37, pp. 174–184, 2018.

[6] S. Chen, D. Yin, F. Cao, Y. Liu, and K. Ren, "An overview of integrated surface subsidence-reducing technology in mining areas of China," *Natural Hazards*, vol. 81, no. 2, pp. 1129–1145, 2016.

[7] J. W. LaMoreaux, Q. Wu, and Z. Wanfang, "New development in theory and practice in mine water control in China," *Carbonates and Evaporites*, vol. 29, no. 2, pp. 141–145, 2014.

[8] H. Yin, Y. Shi, H. Niu et al., "A GIS-based model of potential groundwater yield zonation for a sandstone aquifer in the Juye Coalfield, Shangdong, China," *Journal of Hydrology*, vol. 557, pp. 434–447, 2018.

[9] Y. F. Zeng, Q. Wu, X. Du et al., "Further research on 'water-richness index method' for evaluation of aquifer water abundance," *Journal of China Coal Society*, vol. 45, no. 7, pp. 2423–2431, 2020.

[10] S. P. Neuman, "On methods of determining specific yield," *Ground Water*, vol. 25, no. 6, pp. 679–684, 1987.

[11] W. C. Walton and C. F. McLane, "Aspects of groundwater supply sustainable yield," *Ground Water*, vol. 51, no. 2, pp. 158–160, 2013.

[12] H. Nampak, B. Pradhan, and M. A. Manap, "Application of GIS based data driven evidential belief function model to predict groundwater potential zonation," *Journal of Hydrology*, vol. 513, pp. 283–300, 2014.

[13] P. Sander, M. M. Chesley, and T. B. Minor, "Groundwater assessment using remote sensing and GIS in a rural groundwater project in Ghana: lessons learned," *Hydrogeology Journal*, vol. 4, no. 3, pp. 40–49, 1996.

[14] R. Dhakate, D. K. Chowdhary, V. V. S. Gurunadha Rao, R. K. Tiwary, and A. Sinha, "Geophysical and geomorphological approach for locating groundwater potential zones in Sukinda chromite mining area," *Environmental Earth Sciences*, vol. 66, no. 8, pp. 2311–2325, 2012.

[15] Y. LI, J. YANG, Z. PAN, S. MENG, K. WANG, and X. NIU, "Unconventional natural gas accumulations in stacked deposits: a discussion of upper Paleozoic coal-bearing strata in the east margin of the Ordos basin, China," *Acta Geologica Sinica - English Edition*, vol. 93, no. 1, pp. 111–129, 2019.

[16] Y. Li, D. Z. Tang, X. Hao, D. Elsworth, and Y. J. Meng, "Geological and hydrological controls on water coproduced with coalbed methane in Liulin, eastern Ordos basin, China," *AAPG Bulletin*, vol. 99, no. 2, pp. 207–229, 2015.

[17] Y. Li, Y. B. Wang, J. Wang, and Z. J. Pan, "Variation in permeability during CO_2-CH_4 displacement in coal seams: part 1 - experimental insights," *Fuel*, vol. 263, article 116666, 2020.

[18] M. Qiu, F. J. Huang, Y. Wang, and T. Guan, "Prediction model of water yield property based on GRA, FAHP and TOPSIS methods for Ordovician top aquifer in the Xinwen coalfield of China," *Environmental Earth Sciences*, vol. 79, no. 10, 2020.

[19] Q. Wu, Z. L. Fan, S. Q. Liu, Y. W. Zhang, and W. J. Sun, "Water-richness evaluation method of water-filled aquifer based on the principle of information fusion with GIS: water-richness index method," *Journal of China Coal Society*, vol. 36, no. 7, pp. 1124–1128, 2011.

[20] T. L. Saaty, *The Analytic Hierarchy Process: Planning, Priority Setting, Resource Allocation*, McGraw-Hill, New York, USA, 1980.

[21] L. Q. Shi, M. Qiu, Y. Wang, X. Qu, and T. Liu, "Evaluation of water inrush from underlying aquifers by using a modified water-inrush coefficient model and water-inrush index model: a case study in Feicheng coalfield, China," *Hydrogeology Journal*, vol. 27, no. 6, pp. 2105–2119, 2019.

[22] Q. Wu, K. Xu, W. Zhang, and Z. Wei, "Roof aquifer water abundance evaluation: a case study in Taigemiao, China," *Arabian Journal of Geosciences*, vol. 10, no. 11, 2017.

[23] H. J. Gong, S. L. Liu, and Y. F. Zeng, "Evaluation researchon water-richness of aquifer based on BP artificial neural network," *Coal Technology*, vol. 37, no. 9, pp. 181-182, 2018.

[24] L. M. Fan, L. Q. Ma, Y. H. Yu, S. Wang, and Y. Xu, "Water-conserving mining influencing factors identification and weight determination in northwest China," *International Journal of Coal Science and Technology*, vol. 6, no. 1, pp. 95–101, 2019.

[25] W. Zhai, W. Li, Y. Huang et al., "A case study of the water abundance evaluation of roof aquifer based on the development height of water-conducting fracture zone," *Energies*, vol. 13, no. 16, p. 4095, 2020.

[26] L. L. Xiao, Q. Wu, C. Niu et al., "Application of a new evaluation method for floor water inrush risk from the Ordovician fissure confined aquifer in Xiayukou coal mine, Shanxi, China," *Carbonates and Evaporites*, vol. 35, no. 3, 2020.

[27] Y. Li and M. Song, "Coal mine safety evaluation with V-fold cross-validation and BP neural network," *Journal of Computers*, vol. 5, no. 9, 2010.

[28] Y. Wang, W. F. Yang, M. Li, and X. Liu, "Risk assessment of floor water inrush in coal mines based on secondary fuzzy comprehensive evaluation," *International Journal of Rock Mechanics and Mining Sciences*, vol. 52, pp. 50–55, 2012.

[29] B. Li, Q. Wu, and Z. Liu, "Identification of mine water inrush source based on PCA-FDA: Xiandewang coal mine case," *Geofluids*, vol. 2020, Article ID 2584094, 8 pages, 2020.

[30] W. T. Liu, Q. Li, J. Y. Zhao, and B. Fu, "Assessment of water inrush risk using the principal component logistic regression model in the Pandao coal mine, China," *Arabian Journal of Geosciences*, vol. 11, no. 16, 2018.

[31] H. S. Tian, Y. Q. Hong, and Y. J. Ma, "Hydrogeology characteristics and measures of water prevention in Donghuantuo mine in Kailuan," *Ground Water*, vol. 31, no. 3, pp. 110–113, 2009.

[32] Z. Yang, W. P. Li, J. H. He, and Y. Liu, "An assessment of water yield properties for weathered bedrock zone in Northern Shaanxi Jurassic coalfield: a case study in Jinjitan coal mine, Western China," *Arabian Journal of Geosciences*, vol. 12, no. 23, 2019.

[33] M. Hayaty, M. R. Tavakoli Mohammadi, A. Rezaei, and M. R. Shayestehfar, "Risk assessment and ranking of metals using FDAHP and TOPSIS," *Mine Water and the Environment*, vol. 33, no. 2, pp. 157–164, 2014.

[34] X. Li, "Topsis model with entropy weight for eco geological environmental carrying capacity assessment," *Microprocessors and Microsystems*, vol. 82, article 103805, 2021.

[35] E. Hou, Z. Ji, X. Che et al., "Water abundance prediction method of weathered bedrock based on improved AHP and the entropy weight method," *Journal of China Coal Society*, vol. 44, no. 10, pp. 3164–3173, 2019.

[36] I. Chenini, A. B. Mammou, and M. el May, "Groundwater recharge zone mapping using GIS–based multi-criteria analysis: a case study in Central Tunisia (Maknassy Basin)," *Water Resources Management*, vol. 24, no. 5, pp. 921–939, 2010.

[37] N. S. Magesh, N. Chandrasekar, and J. P. Soundranayagam, "Delineation of groundwater potential zones in Theni district, Tamil Nadu, using remote sensing, GIS and MIF techniques," *Geoscience Frontiers*, vol. 3, no. 2, pp. 189–196, 2012.

[38] I. Park, Y. Kim, and S. Lee, "Groundwater productivity potential mapping using evidential belief function," *Groundwater*, vol. 52, no. S1, pp. 201–207, 2014.

[39] State Administration of Work Safety, State Administration of Coal Mine Safety, *Regulations for Mine Water Prevention and Control*, China Coal Industry Publishing House, Beijing, China, 2009.

[40] K. A. N. Adiat, M. N. M. Nawawi, and K. Abdullah, "Assessing the accuracy of GIS-based elementary multi criteria decision analysis as a spatial prediction tool - a case of predicting potential zones of sustainable groundwater resources," *Journal of Hydrology*, vol. 440-441, pp. 75–89, 2012.

[41] W. J. Guo, J. H. Zhao, L. M. Yin, and D. Kong, "Simulating research on pressure distribution of floor pore water based on fluid-solid coupling," *Arabian Journal of Geosciences*, vol. 10, no. 1, 2017.